Published in final edited form as:
Biochemistry. 2013 July 9; 52(27): 4687–4696. doi:10.1021/bi400540m.

Conserved Hydrogen Bonding Networks of MitoNEET Tune FeS Cluster Binding and Structural Stability

Daniel W. Bak[‡] and **Sean J. Elliott**[§,*]

[‡]Program in Molecular, and Cellular Biology, and Biochemistry, Boston University, Boston, MA 02215

[§]Department of Chemistry, Boston University, Boston, MA 02215

Abstract

While its biological function remains unclear, the 3-Cys, 1-His ligated human [2Fe-2S] cluster containing protein mitoNEET is of interest due to its interaction with the anti-diabetes drug pioglitazone. The mitoNEET [2Fe-2S] cluster demonstrates proton coupled-electron transfer (PCET) and marked cluster instability which have both been linked to the single His-ligand. Highly conserved hydrogen bonding networks, which include the His-87 ligand, exist around the [2Fe-2S] cluster. Through a series of site-directed mutations the PCET of the cluster has been examined, demonstrating that multiple sites of protonation exist in addition to the His-ligand, which can influence redox potential. The mutations also demonstrate that while replacement of the His-ligand with cysteine results in a stable cluster, the removal of Lys-55 also greatly stabilizes the cluster. We have also noted for the first time that the oxidation state of the cluster controls stability; the reduced cluster is stable, while the oxidized one is much more labile. Finally, it is shown that upon cluster loss the mitoNEET protein structure becomes less stable, while upon *in vitro* reconstitution both cluster and secondary structure are recovered. Recently two other proteins have been identified with a 3-Cys(sulfur) 1-His motif, IscR and Grx3/4-Fra2, both of which are sensors of iron and redox homeostatsis. These results lead to a model in which mitoNEET could sense cellular oxidation state and proton concentration and respond through cluster loss and unfolding.

Keywords

MitoNEET; iron-sulfur protein; protein film voltammetry (PFV); proton coupled-electron transfer (PCET); Circular Dichroism (CD)

MitoNEET, a human [2Fe-2S] cluster binding protein (1), was identified in 2004 as a binding target of pioglitazone (2), a thiazolidinedione (TZD) family drug currently on the market to treat Type II Diabetes. MitoNEET is a small 12 kDa protein, that exists as a dimer (1, 3, 4) (Figure 1A), tethered to the cytosolic face of the outer mitochondrial membrane (OMM) by an N-terminal helix (1, 5, 6). Each protomer binds one [2Fe-2S] cluster, the first known OMM protein to do so. There is limited understanding of the role of this protein *in*

[*]Corresponding Author: To whom correspondence should be addressed: Sean J. Elliott, Department of Chemistry, Boston University, 590 Commonwealth Ave., Boston, MA, USA, 02215, Tel.: (617) 358-2816; Fax: (617) 353-6466; elliott@bu.edu.

Author Contributions: The manuscript was written through contributions of all authors. All authors have given approval to the final version of the manuscript.

Supporting Information. Raw PFV data and circular dichroism detected protein stability studies. This material is available free of charge via the Internet at http://pubs.acs.org.

vivo, though roles in iron-sulfur biogenesis (7), iron trafficking (8), redox signaling (9), bioenergetics (5, 10), and cell death and autophagy (11-13) have all been suggested.

The mitoNEET [2Fe-2S] cluster is uniquely ligated by three cysteine residues and a single histidine residue (1). The mitoNEET family of proteins was the first known to have this type of cluster ligation, differing from the all cysteine ligation of classical ferredoxins and the 2-His, 2-Cys ligation of Rieske clusters. It has been shown by our lab and others that several of the unusual properties of mitoNEET displays are the result of this unique histidine ligand (14-17). The ε-nitrogen of the His-ligand (His-87) may be protonated in the course of proton coupled-electron transfer (PCET) chemistry of the mitoNEET cluster. The same protonation also appears to confer pH-dependent instability to the FeS cluster. Replacement of His-87 with a cysteine ligand results in a bound cluster ligated by four cysteine ligands, but with drastically different PCET properties and a greater stability (14, 15).

Interestingly, the His-87 ligand appears to be a part of a more extensive series of hydrogen bonding interactions within the mitoNEET dimer, illustrated by Figure 1. In particular, a lysine residue of the opposite protomer (Figure 1B, C), Lys-55, is conserved in higher eukaryotes, suggesting a conservation of this hydrogen bonding network. Additional H-bond interactions can be seen to exist between the conserved residues Asp-84 and Ser-77, where Asp-84 appears to interact directly with one of the μ-sulfido ligands of the cluster (Figure 1B). Once again these residues are absolutely conserved in mitoNEET homologs. Little attention has been given to the role of these conserved residues in PCET and cluster lability.

Here we have examined how His-87, Lys-55, Asp-84, and Ser-77 all contribute to the overall pH-dependence of the midpoint potential and cluster loss. In both cases it is clear that while the His-87 ligand is important, Lys-55 and to a lesser extent the Asp-84 and Ser-77 residues also play important roles in PCET and pH- and redox-induced cluster loss. We also report the first quantitative redox-dependence of cluster loss, in which the oxidized cluster is significantly less stable than the reduced cluster. Additionally, we see pH-dependent protein structural instability as monitored by circular dichroism, which is strongly affected by replacement of the His-ligand. These results help construct more detailed models of the interplay between mitoNEET protonation, cluster loss, and structural stability, which helps support a protein function in either cluster transfer or redox sensing.

Experimental Procedures

MitoNEET Construct and Mutagenesis

A truncated version of human mitoNEET, without the N-terminal 32 amino acid transmembrane helix was codon-optimized for expression in *E. coli* by Genscript (GenScript Corporation, Piscatway, NJ, USA; www.genscript.com). The gene was supplied in pUC57 with BamHI and SalI cloning sites. MitoNEET-pUC57 was digested with BamHI and SalI and the mitoNEET insert was sub-cloned into pGEX-4T-3 (GE Healthcare), containing an N-terminal GST-tag followed by a thrombin cleavage site (LVPRGS-). Correct ligation of the mitoNEET insert into the pGEX-4T-3 vector was confirmed by sequencing (GeneWiz).

The mitoNEET-pGEX-4T-3 plasmid was used as a template for generating four mitoNEET point mutants (H87C, K55I, D84N, and S77A) and two double mutants (H87C/K55I, and H87C/D84N). Site-directed mutagenesis was preformed using the QuikChange® Lightning site directed mutagenesis kit (Stratagene), with the following primers:

replacement of His-87 by cysteine (H87C) -- 5′-C C G T T T T G C G A T G G C G C G T G T A C C A A A C A T A A C G A A G A A C-3′ & 5′-G T T T C T T C G T T A T G T T T G G T A C A C G C G C C A T C G C A A A A C G G-3′

replacement of Lys-55 by isoleucine (K55I) -- 5′-G C A T A T T C A G A A A G A T A A C C C G A T A A T T G T G C A T G C G T T T G A T A T G G-3′ & 5′-C C A T A T C A A A C G C A T G C A C A A T T A T C G G G T T A T C T T T C T G A A T A T G C-3′,

replacement of Asp-84 by asparagine (D84N) -- 5′-C A A A A A A T T T C C G T T T T G C A A T G G C G C G C A T A C C A A A C-3′ & 5′-G T T T G G T A T G C G C G C C A T T G C A A A A C G G A A A T T T T T T G-3′

replacement of Ser-77 by alanine (S77A) -- 5′-G T A T T G C C G T T G C T G G C G T G C C A A A A A A T T T C C G T T T T G C G-3′ & 5′-C G C A A A A C G G A A A T T T T T T G G C A C G C C A G C A A C G G C A A T A C-3′.

The double mutants were generated by second round of site-directed mutagenesis on the H87C mitoNEET-pGEX-4T-3 plasmid using either the K55I primers or the following new H87C/D84N primers, respectively:

5′-C A A A A A A T T T C C G T T T T G C A A T G G C G C G T G T A C C A A A C-3′ & 5′-G T T T G G T A C A C G C G C C A T T G C A A A A C G G A A A T T T T T T G-3′

All mutations were confirmed via sequencing of the variant mitoNEET-pGEX-4T-3 construct (GeneWiz).

MitoNEET Over-Expression and Purification

Recombinant wild-type mitoNEET and the mitoNEET variants were expressed from the pGEX-4T-3 (AmpR) vector in BL21(DE3) cells with the addition of 0.1 mM IPTG. Cells were grown aerobically overnight at room temperature in 2xYT media with the addition of 1g ferrous ammonium sulfate /L of media. Cells were harvested and purified in 1xPBS buffer (pH 8). Both PMSF and DNase I were added to the cell suspension. Lysis was accomplished with the addition of lysozyme and sonication, and after centrifugation at 15,000 × g, the supernatant was retained. The lysate was loaded onto a glutathione-sepharose affinity resin, washed thoroughly and incubated overnight in the presence of thrombin. The cleaved protein was eluted and, as a further purification step, run over a HiPrep 26/60 Sephacryl S-100 HR column attached to a refrigerated ÄKTApurifier FPLC system. Purity was confirmed by SDS-PAGE gel electrophoresis and Coomassie staining.

Protein Film Voltammetry

Electrochemical experiments were performed using a PGSTAT 12 AutoLab (Ecochemie) potentiostat, equipped with FRA and ECD modules. A three electrode configuration was used, containing a platinum wire counter electrode and a saturated calomel reference electrode. Potentials were corrected by +242 mV in order to be reported vs standard hydrogen electrode (SHE). Room temperature cell solutions were used containing 0.1 M NaCl and 5 mM MES, MOPS, TAPS, CHES, and CAPS, with 5 mM sodium acetate added for the H87C data collection. Pyrolytic graphite-edge (PGE) electrodes with a surface area of 1.4 mm^2 were used and protein films were grown on electrodes by directly depositing 5 μL of ∼250 μM protein sample in 50 mM Tris, 100 mM NaCl at pH 8.5 (storage buffer) for approximately 5 minutes, followed by a rinse with distilled water in order to remove excess protein.

As previously reported with wild-type mitoNEET (14), Non-turnover electrochemical signals were generated on the bench-top with argon bubbled through the cell solution to remove excess oxygen. Data was collected at a scan rate of 100 mV/s between potentials of −0.9 V and 0.1 V with a current range of 10 μA using the GPES software package

(Ecochemie). Non-turnover signals were analyzed by subtraction of baseline electrochemical response of the electrode surface from the raw data using the SO AS package (18).

Proton-Coupled Electron Transfer Theory

By varying the pH of the buffer used in the electrochemical cell the proton-dependence of an electrochemical signal can be monitored. As the pH of the buffer solution is raised the midpoint of the redox couple will shift to more negative values if reduction potential is dependent on proton concentration (pH). This shift in reduction potential as a function of pH can be described by a variation of the Nernst Equation (19), Equation 1.

$$E_{m,obs}=E_{acid}+\left(\frac{m}{n}\right)\left(\frac{RT}{F}\right)\mathrm{In}\left[\frac{[H^+]+K_{red}}{[H^+]+K_{ox}}\right] \quad (1)$$

The term (m/n) describes the ratio of the number of protons (m) and electrons (n) involved; K_{red} and K_{ox} are the equilibrium constants for the protonation of the reduced and oxidized species, respectively; E_{acid} describes the reduction potential of the fully protonated species.

[2Fe-2S] Cluster Loss Assay

UV-visible absorption spectra were recorded in a 1 cm path length quartz cuvette at 25 °C on a Cary 50 Bio UV-Visible Spectrophotometer (Varian) equipped with a Cary single cell peltier accessory to control temperature. Full UV-visible spectra (200-800 nm) were recorded automatically at timed intervals. To initiate cluster loss, mitoNEET protein samples were diluted ~10-fold into a 50 mM acetate, 100 mM NaCl buffer of low pH values (4-6), and quickly mixed. For the reduced protein, absolute anaerobic conditions were necessary in order to avoid re-oxidation of the [2Fe-2S] cluster, therefore the assay was performed in a sealed anaerobic quartz cuvette containing argon sparged buffer supplemented with 5 mM ascorbate. The protein sample was pre-reduced with DTT (dithiothreitol) in an anaerobic glovebox, and introduced into the assay using an air-tight syringe. In order to account for the higher initial pH of the protein storage buffer, a final pH value was recorded for each reaction.

The half-life of cluster loss was determined at 336 nm by Equation 2,

$$A_{1/2(336)}=A_{i(336)}-\left(\frac{A_{i(336)}-A_{f(336)}}{2}\right) \quad (2)$$

where $A_{i(336)}$ and $A_{f(336)}$ are the absorbance of the initial time-point and the final time-point, after the reaction had gone to completion. $t_{1/2}$ is the time-point associated with $A_{1/2(336)}$. Data was reported as the average of three experiments, with error reported in both the pH-based and time-based dimensions.

Generation of apo- and reconstituted-mitoNEET

Generation of the apo-form of mitoNEET by the removal of the [2Fe-2S] cluster could be accomplished by dilution of the protein sample into 50mM sodium acetate, 100 mM NaCl pH 4 solution. The pH of the apo-protein sample was increased back to pH 8 for further characterization. Reconstitution of a [2Fe-2S] cluster into mitoNEET was accomplished through a modified *in vitro assay* (20) using the apo-form of the protein as a target. DTT was added to 1 mM, followed by an addition of 100 μM Ferrous ammonium sulfate and 100 μM sodium sulfide. The reaction was allowed to stand for 10 minutes then another 100 μM

each of iron and sulfide was added. This process was repeated once more so that the final concentration of iron and sulfide was 300 μM. The reaction was allowed to sit for an additional 30 min, before it was loaded onto a PD10 desalting column and the protein fractions collected. The success of each individual reaction varied, but would often return at least at minimum a 50% yield of reconstituted protein. This reconstituted-mitoNEET was then used for further characterization.

Size-Exclusion Chromatography

Protein samples were run through a HiPrep 26/60 Sephacryl S-100 HR column, attached to a refrigerated ÄKTApurifier FPLC system. Samples were automatically injected onto the column after equilibration with phosphate buffer (pH 8). Samples were passed through the column in phosphate buffer (pH 8) at a flow rate of 1 mL/min. Protein elution was monitored by the ÄKTApurifier system at 280 nm.

Electron Paramagnetic Resonance

Low temperature (10 K) EPR measurements were made using a Bruker X-band EleXsys E-500 spectrometer equipped with an ESR900 continuous flow liquid helium cryostat. Reduced mitoNEET samples were generated by prior treatment with dithionite. EPR spectra were collected at (9.37 GHz), (2 mW) microwave power, and with a (15 G) modulation amplitude.

Circular Dichroism

Far UV-CD spectra (190-250 nm) were recorded at 20 °C on an Applied Photophysics CS/2 Chirascan circular dichroism spectrometer, equipped with a Peltier temperature controller unit. Using a 0.1 mm path length quartz cuvette, data were collected at 1 nm steps with an averaging time of 5 sec/step. Protein concentrations of 250 uM in 25 mM sodium acetate, 25 mM sodium phosphate, and 50 mM sodium sulfate, pH adjusted with acetic acid, were used for data collection. Temperature melting curves were obtained with the same protein samples used for the Far UV-CD measurements. The temperature was ramped from 20 °C to 90 °C at a rate of 1 °C/min. Data were recorded at 200 nm and 470 nm every 1 °C with an averaging time of 5 s per step.

Results

Production of mitoNEET point-mutants

In order to interrogate the proton-dependent events of cluster reduction and cluster loss, four protonatable residues around the [2Fe-2S] cluster were targeted for site-directed mutations: His-87, Lys-55, Asp-84, and Ser-77. These positions contribute to two putative hydrogen bonding networks leading away from the [2Fe-2S] cluster (Figure 1B). A His-H_2O-Lys hydrogen bonding network is formed by the ε-nitrogen of the His-ligand (His-87), a conserved water molecule, and the amine group of Lys-55, while a second S^{-2}-Asp-Ser network is formed by the more solvent exposed cluster μ-sulfido ligand, the Asp-84 carboxylate, and the Ser-77 hydroxyl group. All site-directed mutations were made with the goal of eliminating the protonation site of the amino acid side chain, while otherwise being as conservative as possible; histidine to cysteine (H87C), lysine to isoleucine (K55I), aspartate to asparagine (D84N), and serine to alanine (S77A).

For convenience of study, mitoNEET's N-terminal 32 amino acids were excluded from the recombinant construct generated for this work. As described for previous mitoNEET constructs, including the crystallographically characterized human (1, 3, 4) and *Arabidopsis*(21) proteins, omission of the N-terminal transmembrane helix resulted in no

obvious deleterious effects on the soluble [2Fe-2S] cluster binding domain (1, 3, 4). All four point-mutants and the H87C/K55I and H87C/D84N double mutants could be readily expressed and easily solubilized. Reconstitution of the [2Fe-2S] cluster prior to further characterization was unnecessary as all mitoNEET variants fully incorporated their cluster when over-expressed in *E. coli*.

Proton coupled-electron transfer at the mitoNEET [2Fe-2S] cluster

Wild-type mitoNEET and site-directed variants were examined using direct electrochemistry with polished pyrolytic graphite edge (PGE) electrodes. For all variants, the voltammetric features were highly reversible: peak separations and widths at half-height are close to those predicted for a simple reversible one-electron process marked by facile interfacial electron transfer and a homogenous protein monolayer (22-24). A Pourbaix plot of reduction potential vs pH provides insight into the proton-dependent nature of the midpoint potential, reported here for mitoNEET and its variants (Figure 2).

We previously reported proton-dependent midpoint potentials for the wild-type protein (14), which displayed an unexpectedly shallow gradient of only -40 mV per decade (Figure 2 - grey squares). This prevented the use of the Nernst equation for a single one-proton, one-electron couple, where the slope of the pH-dependent region is a -60 mV gradient. Instead, Equation 3 was used to models a one-electron process coupled to two distinct protonation events.

$$E_{m,obs}=E_{alk}+\left(\frac{m}{n}\right)\left(\frac{RT}{F}\right)\mathrm{In}\left[\left(1+\frac{[H^+]}{K_{red2}}+\frac{[H^+]^2}{K_{red1}K_{red2}}\right)/\left(1+\frac{[H^+]}{K_{ox2}}+\frac{[H^+]^2}{K_{\mathrm{ox1}}K_{ox2}}\right)\right] \quad (3)$$

As in Equation 1, the term (m/n) describes the ratio of the number of protons (m) and electrons (n) involved and E_{alk} describes the reduction potential of the fully protonated species. K_{red1} and K_{ox1} are the equilibrium constants of the reduced and oxidized species for the first protonation event, while K_{red2} and K_{ox2} are the equilibrium constants for the second protonation event. Unlike Rieske proteins, whose pK_{ox12} *and* $pK_{red1,2}$ values are well separated, resulting in a -120 mV per decade region of two-proton one-electron coupling (25, 26), here the relative order *of* pK_a values differs ($pK_{ox1} < pK_{red1} < pK_{ox2} < pK_{red2}$) resulting in a shallower and more featured potential gradient for the mitoNEET [2Fe-2S] cluster. These two regions of pH-dependence, between pK_{ox1} and pK_{red1} and between pK_{ox2} and pK_{red2} will be referred to as the neutral (6.5 to 9.5) and alkaline (10.0 to 12.5) regions of pH-dependence respectively. The strength of coupling can be established by ΔpK, the difference between pK_{red} and pK_{ox}. For reference, the His-ligands in Reiske proteins display ΔpK values ranging from approximately 2 to 5 (26). Here we continue this analysis using a variety of site-directed mutants aimed at identifying the sites of protonation coupled to electron transfer. Table 1 gathers and compares pK_a, ΔpK, and E_{acid} (the comparative midpoint potential of the fully protonated species) values for all mitoNEET mutants.

Mutation of the His-87 ligand or the Lys-55 residue both significantly change the pH-dependence profiles in terms of the pK_a values and shifts in midpoint potential of the mitoNEET cluster (Figure 2 - black open squares, red solid diamonds). The pH-dependence curves for both mutants share a weakly coupled neutral region of pH-dependence with an approximate ΔpK of 1. Additionally, both mutants contain a more alkaline region of pH-dependence, which is lost in the H87C/K55I double mutant (Figure 2 - red open diamonds). This indicates that the weakly coupled alkaline pH-dependence of the H87C mutant is likely due to the protonation of Lys-55, while the strongly coupled region of pH-dependence in the K55I mutant is the result of His-87 protonation. This alkaline region of pH dependent in the

K55I mutant with a pK_{ox} of 8.71 and a ΔpK of 4.3 is similar to the pH-dependence profile of His-ligands in Rieske proteins (26).

The H87C/D84N double mutant was used (Figure 2 - blue open circles) to test whether the Asp-84 residue could be responsible for the neutral region of pH-dependence seen in the previous mutants. Its pH-dependence profile was similar to the profile for the H87C mutant, indicating that the Asp-84 residue likely is not responsible for the neutral region of pH-dependence. The D84N and S77A mutants show minimal deviations from the wild-type pH-dependence data (Fig. 2 - blue solid circles and green solid triangles), though small changes can be seen for both of these mutations. Specifically the S77A seems to affects the neutral region of pH dependence more strongly than the alkaline one.

These results confirm our earlier model that the pH-dependence of mitoNEET is not a simple one-proton one-electron couple as suggested by others, where an empirical factor was used to fit the pH dependence (27). As shown here, the interdependence of the hydrogen bond networks makes it difficult to assign the two regions of pH-dependence in the wild-type protein, as any change made to the protein by the mutation of residues leads to a shift in the pK_a of the remain residues.

Proton and Redox Dependent Loss of the mitoNEET [2Fe-2S] Cluster

The [2Fe-2S] cluster of wild-type mitoNEET has previously been shown to be unstable below neutral pH, while the H87C mutant has been shown to be resistant to pH-dependent cluster loss (15). Since the His-87 ligand is not the sole determinant of the pH-dependence of the midpoint potential, the additional point mutants (K55I, D84N, and S77A) were examined to identify their affect on the pH dependence of mitoNEET cluster loss. The dependence of cluster loss on redox state has also been examined here. Monitoring the presence of the MitoNEET [2Fe-2S] cluster by optical spectroscopy, we have confirmed reports of the instability of the oxidized wild-type protein at pH 5.20 (Figure 3A). The visible signal intensity (associated with the Fe-cysteinate ligand charge transfer (28)) had decayed to about 50% after 20 minutes, and almost fully within one hour. In contrast, the reduced state of mitoNEET at pH 5.20 is almost completely stable (Figure 3B), with only a slight loss in absorption signal after an hour.

The cluster loss at pH 5.20-5.30 is shown for the wild-type protein and all four point-mutants (Figure 4), with the exception of the H87C mutant which is presented at pH 4.55. The H87C mutant is completely stable over the range of pH values assayed, demonstrating that His-87 is necessary for [2Fe-2S] instability. Using the half-life of the optical signals as a metric for the stability of the [2Fe-2S] cluster illustrates the variation of cluster stability as a function of pH (Figure 5). For example, the K55I mutant has a stabilizing affect on the [2Fe-2S] cluster at pH 5.25 (Figure 4), and it is also clear that removal of the amine group stabilizes the cluster significantly over a range of pH, as evidenced by a shift of the cluster half-life curve (Figure 5 -diamonds). Alternatively, both the D84N and S77A mutants at pH 5.30 (Figure 4) and over a range of pH values (Figure 5 - circles and triangles) are less stable when compared to the wild-type protein. This would suggest that the hydrogen bonding network created by these two residues and the μ-sulfido-ligand has a stabilizing role to play with respect to the cluster.

In vitro Reconstitution of Apo-mitoNEET

To determine, at least *in vitro*, whether cluster loss is a reversible phenomenon, a reconstitution of apo-mitoNEET was performed under anaerobic conditions in an anaerobic glove-box. It was found that using DTT as an electron donor instead of dithionite, and gradually adding small aliquots of Fe^{+2} and S^{-2} resulted in better yields of the reconstituted

protein, as reported previously for human ferredoxin (20). Reconstitution of the native [2Fe-2S] cluster was confirmed spectroscopically: The visible absorption bands associated with both the oxidized (Figure 6A) and reduced (Figure 6A - inset) states of the reconstituted protein match up well to the native form of the protein. Small deviations from the native absorption spectrum are most likely the result of some non-specific FeS binding, but these appear to represent only a minor fraction of the overall sample. Reconstitution of the native cluster was also confirmed with electron paramagnetic resonance (EPR) (Figure 6B). EPR spectra for the reconstituted protein in the reduced state overlays nicely with the reduced native protein, both having *g*-values of 1.94. Oxidized, reconstituted mitoNEET is EPR silent (like native protein, data not shown). It is clear that upon *in vitro* reconstitution, mitoNEET is capable of binding a [2Fe-2S] cluster with the same 3-Cys, 1-His ligand set as the native protein, suggesting that cluster loss is in theory a reversible event.

Structural Instability of Apo-mitoNEET

A significant decrease in the absorbance at 280 nm can be seen upon cluster loss for the wild-type and site-directed variants of mitoNEET (Figure 4). The 280 nm signal is reduced by approximately one-third in the apo-form of the protein as compared to the holo-protein. Each mitoNEET monomer contains one tryptophan residue (Trp-75), which is responsible for the majority of the protein based UV-absorbance around 280 nm. This tryptophan sits at the dimer interface and is buried from solvent exposure. As the optical absorbance of tryptophan can be affected by the local environment, upon loss of cluster, mitoNEET likely undergoes a conformational change that alters the local environment of the tryptophan residue (29). Here, we have examined the impact of cluster loss upon the solution structure of mitoNEET variants in terms of both the quaternary structure of the mitoNEET dimer, and the secondary structure of the protein.

To test whether mitoNEET was undergoing an oligomeric change upon cluster loss, both apo-and holo-mitoNEET were run on an S-100 size-exclusion column. Holo-mitoNEET eluted as only one major species around 20 kDa (Figure 7 - solid trace), representative of the dimeric protein. The apo-protein, after being generated at low pH, eluted as a mixture of higher molecular weight species (Figure 7 - dotted trace). Virtually no dimeric mitoNEET remained, and there was no indication of the monomeric species, suggesting multimerization and/or nonspecific aggregation occurs upon cluster loss.

The far-UV CD spectra of oxidized mitoNEET displays a negative feature centered at 220 nm (Supporting Figure 2) and is suggestive of both α-helical and β-sheet content (30), as would be anticipated for mitoNEET, which contains one 3-strand β-sheet, and two short α-helices per monomer. When mitoNEET is denatured by heating to 90 °C, the negative feature at 220 nm diminishes and overall the negative features between 200 and 230 nm are broadened (Supporting Figure 2). This spectrum is suggested of a molten globule state which has been seen previously for unloaded iron-sulfur proteins (31). Interestingly this state can also be achieved by generating the apo-form of the protein at low pH at 20 °C (Supporting Figure 2), suggesting that pH dependent loss of cluster is concomitant with protein structure destabilization. Here pH appears to be as strong a switch for protein unfolding as heat denaturation is.

To better understand the effect of pH on protein stability, a series of temperature melts were performed with the wild-type, oxidized protein. Additionally, the CD characteristics in the visible region that are due to the presence of the oxidized cluster can similarly monitored at 470 nm (Supporting Figure 3). In Figure 8 the depletion of secondary structure (monitored at 220 nm) as well as the presence of the FeS cluster (monitored at 470 nm) are shown as a function of temperature. At pH 8 (Figure 8, bottom, solid squares) mitoNEET has an apparent melting temperature ($T_{m,app}$) of 75 °C (As this protein unfolding event is not

reversible, true thermodynamic parameters cannot be determined). When unfolding measurements were repeated for mitoNEET at pH 7 and 6 (Figure 8, bottom, half-filled and open squares, respectively), a significant shift was seen in the values of the $T_{m,app}$, lowered to 65 °C for pH 7 and 50 °C for pH 6. The H87C mutant had a $T_{m,app}$ of 70 °C at pH 6 (Figure 8 - bottom panel red open diamonds) indicating a significant increase in protein stability for this mutant. At higher pH values the unfolding of the H87C mutant had not gone to completion by 90 °C, suggesting $T_{m,app}$ greater than 90 °C.

Interestingly, for the wild-type protein loss of the 470 nm signal (Figure 8 - top panel) occurs at approximately the same temperature as $T_{m,app}$ at all pH values. This suggests a strong coupling between loss of cluster and protein unfolding in mitoNEET. Alternatively the loss of cluster in the H87C variant occurs at significantly higher temperatures than its $T_{m,app}$ suggesting that even in the unfolded state the four cysteine ligands of H87C mutant are still ligating the FeS cluster. And at higher pH values, cluster loss of H87C had not fully occurred by 90 °C.

Discussion

A clear picture of the role of mitoNEET has failed to emerge since the identification of this unique [2Fe-2S] cluster binding protein almost 10 years ago. It is presumed that at the heart of whatever biological function mitoNEET may have, the conservation of the cluster's lone ligating histidine (His-87) indicates a crucial role for this residue. Postulated roles in cluster transfer, bioenergetics, and redox sensing have all been put forth as possible functions for mitoNEET, where His-87 may be involved in tuning reduction potential (27), controlling cluster stability (15), and mitigating PCET (14, 27).

Little attention has been given to the fact that other highly conserved non-ligating residues exist around the cluster and participate in conserved hydrogen bonding networks. Lys-55 forms a hydrogen bonding network with His-87 through a conserved water molecule (present in all eukaryotic mitoNEET-like protein crystal structures (1, 3, 4, 21, 32)). This residue, donated from the opposite monomer, crosses the dimer interface, though in some bacterial/archaeal mitoNEET homologs this residue is at the n+1 position to the His-ligand, but still within hydrogen bonding distance to the histidine ε-nitrogen (33). A second conserved hydrogen bond network (between Ser-77, Asp-84 and the more solvent exposed cluster μ-sulfido ligand) is also conserved in all mitoNEET-like structures, with these residues also conserved in all mitoNEET-like sequences. Here, we have elucidated the role of these conserved residues and the affect of their hydrogen bonding networks on PCET and stability of the mitoNEET [2Fe-2S] cluster.

The pH dependence curves for the multiple mitoNEET variants, clearly show the importance of the PCET event associated with His-87, but unlike Rieske proteins where the ε-nitrogen of both His-ligands are solvent exposed (34), here the His-H_2O-Lys network appears to act as a means for proton-coupling to extend from the ligating residue to additional elements of protein structure. It is difficult to assign specific sites of protonation to each region of pH dependence since, for example, mutation of Lys-55 results in a shift in the pK_a values associated with the His-87 ligand. Most likely the more alkaline pH dependence represents a protonation of the His-H_2O-Lys network, while the more neutral region of pH dependence might come from an alternative site. Additional hydrogen bonding networks in the interior of the protein and at the dimer interface, including Arg-73 and His-58 may also be involved in long-range PCET. In the case of some clusters, direct protonation at a μ-sulfido ligand is possible, as described for the [3Fe-4S] cluster of *Azotobacter vinlandeii* Ferredoxin I (AvFdI) (35).

Despite being unable to definitively assign the neutral PCET event, it is possible that it may be responsible for cluster lability, as the cluster becomes highly unstable below neutral pH. Cluster loss is additionally dependent on redox state, indicating a possible role in redox sensing. At physiological pH the cytosolic resting potentials are approximately -290 mV (36), suggesting that mitoNEET ($E_{m,7}$ = 0 mV) would primarily exist in a reduced state, which would be stable to cluster loss. While under oxidative stress conditions or certain physiological conditions such as apoptosis and differentiation (37), where the cytosolic potential could rise as high as +200 mV, the cluster would become oxidized and susceptible to cluster loss.

As indicated by the more stable cluster half-lives of the H87C and K55I mutants, the His-H_2O-Lys hydrogen bonding network plays a significant role in cluster lability. While an argument could be made that cluster instability is tolerated due to the significant increase in midpoint potential afforded by the presence of His-87, the same argument does not hold for the Lys-55 residue. At neutral pH, loss of Lys-55 results in almost no change in redox potential. Thus, the highly conserved nature of this residue suggests that the mitoNEET protein may have evolved this hydrogen bonding network, not to tune reduction potential, but to tune cluster stability. Indeed, protonation of His-87 is likely not a sole determinant of stability: Rieske centers, with two His-ligands, but lacking in the unique His-H_2O-Lys network have never been shown to contain unstable clusters upon protonation of their ligands (38). Together, these observations support the hypothesis that cluster transfer (or loss) due to redox sensing is of potential biological significance, as suggested previously (7).

Here we have demonstrated that the quaternary and secondary structure of MitoNEET itself is intimately tied to whether or not the FeS cluster is bound. It has been noted previously that apoferredoxins adopt a molten globule like state in the absence of their FeS clusters. For example, the [3Fe-4S][4Fe-4S] ferredoxin from *Acidianus ambivalens* (AaFd) (31), retains elements of secondary structural and its compactness is like that of the holo-protein. Additionally, the IscU FeS scaffold proteins from *Escherichia coli* (39-41) and *Thermotoga maritima* (42-44) which only transiently host an FeS cluster, exist as an equilibrium between a more structured state and a disordered state in the absence of cluster. Yet, the apparent lability of the MitoNEET FeS cluster may not entirely indicate a role for cluster transfer: the CD spectra of both the thermal- and pHunfolded state of mitoNEET are not suggestive of proteins with a random coil structure, suggesting that a degree of secondary structure remains. Additionally the $T_{m,app}$ of both unfolding and cluster loss in the mitoNEET protein at neutral pH is much more comparable to those calculated for ferredoxin proteins (between 60 and 80 °C). For IscU-like proteins the temperature associated with cluster loss is approximately 40 °C (43). Interestingly, at lower pH the unfolding and cluster loss of mitoNEET more closely matches what is seen in IscU-like proteins. This could suggest that while the mitoNEET [2Fe-2S] cluster is not as transient as those seen in IscU type proteins, under certain conditions the structural flexibility of the protein could enhance cluster transfer.

The mitoNEET homolog, miner1 has been shown to interact with Beclin1/Bcl-2 at the ERcytosolic interface in order to inhibit signaling for autophagy but is incapable of protein interactions in the absence of cluster (11)(13). This observation is easily explained if apo-miner1 is as structurally flexible as mitoNEET. This would be an intriguing and unique mechanism for signaling within cells; disruption of FeS cluster binding leading to a less structurally stable protein, results in a loss of protein-protein interactions leading to downstream signaling effects. While the native protein partners of mitoNEET are unknown it will be interesting to see under what conditions mitoNEET may be able to interact with them.

Recently two other proteins have been identified with putative 3-sulfur (Cys, glutathione), 1-His ligand sets, where cluster lability is potentially significant to function: the bacterial transcription factor IscR (45), and the iron-regulatory proteins Grx3/4 and Fra2 in yeast (46) and Glrx3 and BolA2 in humans (47). *E. coli* IscR plays a role in FeS biogenesis as a sensor of the need for FeS cluster production (48). In yeast, cytosolic monothiol glutaredoxins (Grx3 and Grx4) interact with Fra2 to form a [2Fe-2S] at the dimer interface, which prevents activation of the Atf1/2 transcription factor and transcription of the iron regulon (49). This interaction appears to be conserved in mammals, with Glrx3 and BolA2 interacting in a similar manner. Interestingly, IscR and Grx3/4-Fra2 both play a role in sensing iron need within the cell and likely cluster loss prevents interactions with either DNA or proteins, respectively. The fact that these proteins, along with mitoNEET, possibly each ligate a [2Fe-2S] cluster, with a single His-ligand suggest that perhaps this ligation motif represents a functional strategy for sensing iron and redox homeostasis within a cell, however, the -redox-dependent properties of these novel Cys/His ligated FeS clusters have been largely unexplored.

Conclusion

This study demonstrates that mitoNEET responds to both lowered pH and increased oxidative stress with the loss of its [2Fe-2S] cluster. This cluster loss is concomitant with loss of structural stability, but cluster assembly and protein refolding is facile. We believe this work will potentially direct future biological studies of the functional role of mitoNEET, whether that be redox sensing, cluster transfer, or some unknown role.

Supplementary Material

Refer to Web version on PubMed Central for supplementary material.

Acknowledgments

Funding Sources: This work has been kindly supported by NIH grant R01 GM072663 to S.J.E. and NSF grants CHE 0840418 and MCB 1122977.

References Cited

1. Paddock ML, Wiley SE, Axelrod HL, Cohen AE, Roy M, Abresch EC, Capraro D, Murphy AN, Nechushtai R, Dixon JE. MitoNEET is a uniquely folded 2Fe–2S outer mitochondrial membrane protein stabilized by pioglitazone. Proceedings of the National Academy of Sciences. 2007; 104:14342–14347.
2. Colca JR, McDonald WG, Waldon DJ, Leone JW, Lull JM, Bannow CA, Lund ET, Mathews WR. Identification of a novel mitochondrial protein (“ mitoNEET”) cross-linked specifically by a thiazolidinedione photoprobe. American Journal of Physiology-Endocrinology And Metabolism. 2004; 286:E252–E260. [PubMed: 14570702]
3. Lin J, Zhou T, Ye K, Wang J. Crystal structure of human mitoNEET reveals distinct groups of iron–sulfur proteins. Proceedings of the National Academy of Sciences. 2007; 104:14640–14645.
4. Hou X, Liu R, Ross S, Smart EJ, Zhu H, Gong W. Crystallographic studies of human MitoNEET. J Biol Chem. 2007; 282:33242–33246. [PubMed: 17905743]
5. Wiley SE, Murphy AN, Ross SA, Van Der Geer P, Dixon JE. MitoNEET is an iron-containing outer mitochondrial membrane protein that regulates oxidative capacity. Proceedings of the National Academy of Sciences. 2007; 104:5318–5323.
6. Wiley SE, Rardin MJ, Dixon JE. Localization and Function of the 2Fe-2S Outer Mitochondrial Membrane Protein mitoNEET. Methods Enzymol. 2009; 456:233–246. [PubMed: 19348892]
7. Zuris JA, Harir Y, Conlan AR, Shvartsman M, Michaeli D, Tamir S, Paddock ML, Onuchic JN, Mittler R, Cabantchik ZI. Facile transfer of [2Fe-2S] clusters from the diabetes drug target

mitoNEET to an apo-acceptor protein. Proceedings of the National Academy of Sciences. 2011; 108:13047–13052.

8. Kusminski CM, Holland WL, Sun K, Park J, Spurgin SB, Lin Y, Askew GR, Simcox JA, McClain DA, Li C, Scherer PE. MitoNEET-driven alterations in adipocyte mitochondrial activity reveal a crucial adaptive process that preserves insulin sensitivity in obesity. Nat Med. 2012; 18:1539–1549. [PubMed: 22961109]
9. Zhou T, Lin J, Feng Y, Wang J. Binding of NADPH destabilizes the ironsulfur clusters of human mitoNEET. Biochemistry. 2010; 49(44):9604–9612. [PubMed: 20932062]
10. Tsai, TF.; Chen, YF.; Tsai…, SF. CISD2-Knockout Mice and Uses Thereof. US Patent App. 12/481. 2009.
11. Maiuri MC, Criollo A, Kroemer G. Crosstalk between apoptosis and autophagy within the Beclin 1 interactome. The EMBO journal. 2010; 29:515–516. [PubMed: 20125189]
12. Chen YF, Wu CY, Kirby R, Kao CH, Tsai TF. A role for the CISD2 gene in lifespan control and human disease. Ann N Y Acad Sci. 2010; 1201:58–64. [PubMed: 20649540]
13. Chang NC, Nguyen M, Germain M, Shore GC. Antagonism of Beclin 1-dependent autophagy by BCL-2 at the endoplasmic reticulum requires NAF-1. The EMBO journal. 2009; 29:606–618. [PubMed: 20010695]
14. Bak DW, Zuris JA, Paddock ML, Jennings PA, Elliott SJ. Redox characterization of the FeS protein MitoNEET and impact of thiazolidinedione drug binding. Biochemistry. 2009; 48:10193–10195. [PubMed: 19791753]
15. Wiley SE, Paddock ML, Abresch EC, Gross L, van der Geer P, Nechushtai R, Murphy AN, Jennings PA, Dixon JE. The outer mitochondrial membrane protein mitoNEET contains a novel redox-active 2Fe-2S cluster. J Biol Chem. 2007; 282:23745–23749. [PubMed: 17584744]
16. Iwasaki T, Samoilova RI, Kounosu A, Ohmori D, Dikanov SA. Continuous-Wave and Pulsed EPR Characterization of the [2Fe– 2S](Cys) 3 (His) 1 Cluster in Rat MitoNEET. J Am Chem Soc. 2009; 131:13659–13667. [PubMed: 19736979]
17. Dicus MM, Conlan A, Nechushtai R, Jennings PA, Paddock ML, Britt RD, Stoll S. Binding of Histidine in the (Cys) 3 (His) 1-Coordinated [2Fe– 2S] Cluster of Human mitoNEET. J Am Chem Soc. 2010; 132:2037–2049. [PubMed: 20099820]
18. Fourmond V, Hoke K, Heering HA, Baffert C, Leroux F, Bertrand P, Léger C. SOAS: A free program to analyze electrochemical data and other one-dimensional signals. Bioelectrochemistry. 2009; 76:141–147. [PubMed: 19328046]
19. Clark, WM.; Clark, WM. Oxidation-reduction potentials of organic systems. Vol. 1960. The Williams & Wilkins Company; Baltimore: 1960.
20. Coghlan VM, Vickery LE. Site-specific mutations in human ferredoxin that affect binding to ferredoxin reductase and cytochrome P450scc. J Biol Chem. 1991; 266:18606–18612. [PubMed: 1917982]
21. Nechushtai R, Conlan AR, Harir Y, Song… L. Characterization of Arabidopsis NEET Reveals an Ancient Role for NEET Proteins in Iron Metabolism. The Plant Cell. 2012; 24(5):2139–2154. [PubMed: 22562611]
22. Léger C, Elliott SJ, Hoke KR, Jeuken LJC, Jones AK, Armstrong FA. Enzyme electrokinetics: Using protein film voltammetry to investigate redox enzymes and their mechanisms. Biochemistry. 2003; 42:8653–8662. [PubMed: 12873124]
23. Armstrong F. Probing metalloproteins by voltammetry. Bioinorganic Chemistry. 1990:137–221.
24. Armstrong FA, Heering HA, Hirst J. Reaction of complex metalloproteins studied by protein-film voltammetry. Chem Soc Rev. 1997; 26:169–179.
25. Zu Y, James A, Hirst J. Complete thermodynamic characterization of reduction and protonation of the bc 1-type Rieske [2Fe-2S] center of Thermus thermophilus. J Am Chem Soc. 2001; 123:9906–9907. [PubMed: 11583559]
26. Zu Y, Manon MJC, Kolling DRJ, Antony R, Eltis LD, James A, Hirst J. Reduction potentials of Rieske clusters: importance of the coupling between oxidation state and histidine protonation state. Biochemistry. 2003; 42:12400–12408. [PubMed: 14567701]

27. Zuris JA, Halim DA, Conlan AR, Abresch EC, Nechushtai R, Paddock ML, Jennings PA. Engineering the redox potential over a wide range within a new class of FeS proteins. J Am Chem Soc. 2010; 132(38):13120–13122. [PubMed: 20812736]
28. Noodleman L, Norman JG Jr, Osborne JH, Aizman A, Case DA. Models for ferredoxins: electronic structures of iron-sulfur clusters with one, two, and four iron atoms. J Am Chem Soc. 1985; 107:3418–3426.
29. Lin SW, Sakmar TP. Specific tryptophan UV-absorbance changes are probes of the transition of rhodopsin to its active state. Biochemistry. 1996; 35:11149–11159. [PubMed: 8780519]
30. Johnson WCJ. Secondary structure of proteins through circular dichroism spectroscopy. Annu Rev Biophys Biophys Chem. 1988; 17:145–166. [PubMed: 3293583]
31. Leal SS, Gomes CM. Studies of the molten globule state of ferredoxin: structural characterization and implications on protein folding and iron-sulfur center assembly. Proteins. 2007; 68:606–616. [PubMed: 17510960]
32. Conlan AR, Axelrod HL, Cohen AE, Abresch EC, Zuris J, Yee D, Nechushtai R, Jennings PA, Paddock ML. Crystal structure of Miner1: The redox-active 2Fe-2S protein causative in Wolfram Syndrome 2. J Mol Biol. 2009; 392:143–153. [PubMed: 19580816]
33. Lin J, Zhang L, Lai S, Ye K. Structure and Molecular Evolution of CDGSH Iron-Sulfur Domains. PloS one. 2011; 6:e24790. [PubMed: 21949752]
34. Hunsicker-Wang LM, Heine A, Chen Y, Luna EP, Todaro T, Zhang YM, Williams PA, McRee DE, Hirst J, Stout CD. High-resolution structure of the soluble, respiratory-type Rieske protein from Thermus thermophilus: analysis and comparison. Biochemistry. 2003; 42:7303–7317. [PubMed: 12809486]
35. Camba R, Jung YS, Hunsicker-Wang LM, Burgess BK, Stout CD, Hirst J, Armstrong FA. Mechanisms of redox-coupled proton transfer in proteins: role of the proximal proline in reactions of the [3Fe-4S] cluster in Azotobacter vinelandii ferredoxin I. Biochemistry. 2003; 42:10589–10599. [PubMed: 12962482]
36. Hu J, Dong L, Outten CE. The redox environment in the mitochondrial intermembrane space is maintained separately from the cytosol and matrix. J Biol Chem. 2008; 283:29126–29134. [PubMed: 18708636]
37. Hansen JM, Go YM, Jones DP. Nuclear and mitochondrial compartmentation of oxidative stress and redox signaling. Annu Rev Pharmacol Toxicol. 2006; 46:215–234. [PubMed: 16402904]
38. Schröter T, Hatzfeld OM, Gemeinhardt S, Korn M, Friedrich T, Ludwig B, Link TA. Mutational analysis of residues forming hydrogen bonds in the Rieske [2Fe-2S] cluster of the cytochrome bc1 complex in Paracoccus denitrificans. Eur J Biochem. 1998; 255:100–106. [PubMed: 9692907]
39. Kim JH, Fuzery AK, Tonelli M, Ta DT, Westler WM, Vickery LE, Markley JL. Structure and dynamics of the iron-sulfur cluster assembly scaffold protein IscU and its interaction with the cochaperone HscB. Biochemistry. 2009; 48:6062–6071. [PubMed: 19492851]
40. Kim JH, Tonelli M, Markley JL. Disordered form of the scaffold protein IscU is the substrate for iron-sulfur cluster assembly on cysteine desulfurase. Proc Natl Acad Sci U S A. 2012; 109:454–459. [PubMed: 22203963]
41. Adinolfi S, Rizzo F, Masino L, Nair M, Martin SR, Pastore A, Temussi PA. Bacterial IscU is a well folded and functional single domain protein. Eur J Biochem. 2004; 271:2093–2100. [PubMed: 15153099]
42. Bertini I, Cowan JA, Del Bianco C, Luchinat C, Mansy SS. Thermotoga maritima IscU. Structural characterization and dynamics of a new class of metallochaperone. J Mol Biol. 2003; 331:907–924. [PubMed: 12909018]
43. Mansy SS, Wu G, Surerus KK, Cowan JA. Iron-sulfur cluster biosynthesis. Thermatoga maritima IscU is a structured iron-sulfur cluster assembly protein. J Biol Chem. 2002; 277:21397–21404. [PubMed: 11934893]
44. Mansy SS, Wu SP, Cowan JA. Iron-sulfur cluster biosynthesis: biochemical characterization of the conformational dynamics of Thermotoga maritima IscU and the relevance for cellular cluster assembly. J Biol Chem. 2004; 279:10469–10475. [PubMed: 14688265]

45. Fleischhacker AS, Stubna A, Hsueh KL, Guo Y, Teter SJ, Rose JC, Brunold TC, Markley JL, Münck E, Kiley PJ. Characterization of the [2Fe-2S] Cluster of Escherichia coli Transcription Factor IscR. Biochemistry. 2012; 51(22):4453–4462. [PubMed: 22583201]

46. Li H, Mapolelo DT, Dingra NN, Naik SG, Lees NS, Hoffman BM, Riggs-Gelasco PJ, Huynh BH, Johnson MK, Outten CE. The yeast iron regulatory proteins Grx3/4 and Fra2 form heterodimeric complexes containing a [2Fe-2S] cluster with cysteinyl and histidyl ligation. Biochemistry. 2009; 48:9569–9581. [PubMed: 19715344]

47. Li H, Mapolelo DT, Randeniya S, Johnson MK, Outten CE. Human Glutaredoxin 3 Forms [2Fe-2S]-Bridged Complexes with Human BolA2. Biochemistry. 2012; 51(8):1687–1696. [PubMed: 22309771]

48. Giel JL, Rodionov D, Liu M, Blattner FR, Kiley PJ. IscR-dependent gene expression links iron-sulphur cluster assembly to the control of O2-regulated genes in Escherichia coli. Mol Microbiol. 2006; 60:1058–1075. [PubMed: 16677314]

49. Li H, Outten CE. Monothiol CGFS Glutaredoxins and BolA-like Proteins:[2Fe-2S] Binding Partners in Iron Homeostasis. Biochemistry. 2012; 51(22):4377–4389. [PubMed: 22583368]

Abbreviations

CAPS	N-cyclohexyl-3-aminopropanesulfonic Acid
CD	Circular Dichroism
CHES	2-(Cyclohexylamino)ethanesulfonic Acid
DNaseI	Deoxyribonuclease I
DTT	Dithiothritol
EPR	Electron Paramagnetic Resonance
ER	Endoplasmic Reticulum
FPLC	Fast Protein Liquid Chromatography
IPTG	Isopropyl b-D-1-thiogalactopyranoside
OMM	Outer Mitochondrial Membrane
PBS	Phosphate Buffered Saline
MES	2-(N-morpholino)ethanesulfonic Acid
MOPS	3-(N-morpholino)propanesulfonic Acid
PCET	Proton Coupled-Electron Transfer
PFV	Protein Film Voltammetry
PMSF	Phenylmethanesulfonyl Fluoride
TAPS	3-[[1,3-dihydroxy-2-(hydroxymethyl)propan-2-yl]amino]propane-1-sulfonic Acid
TZD	Thiazolidinedione

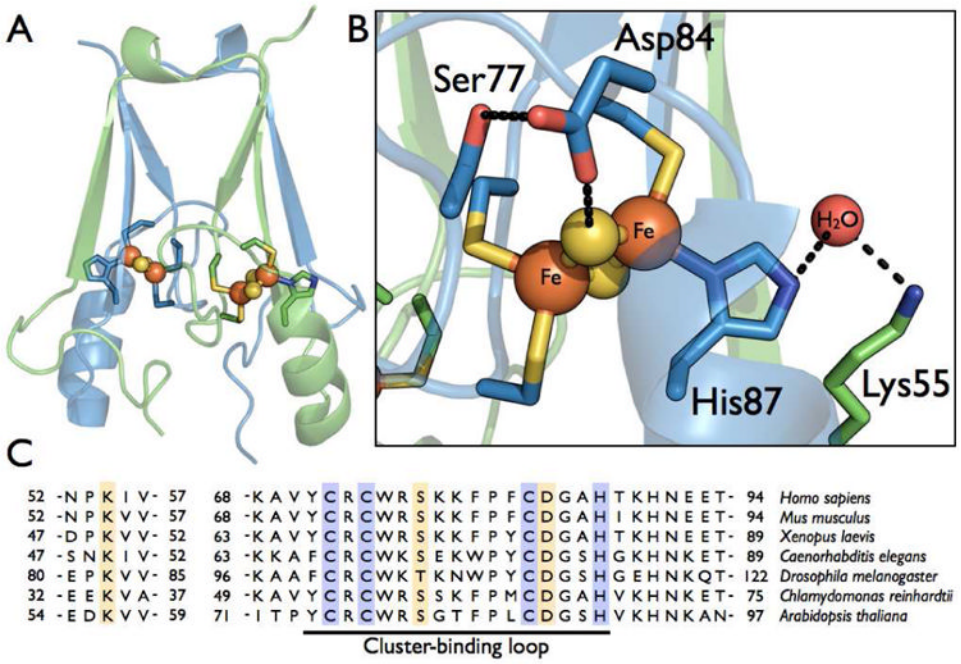

Figure 1.

Structure and sequence comparison of human mitoNEET. (A) The dimeric mitoNEET protein is displayed with each monomer (colored blue or green) containing one [2Fe-2S] cluster, ligated by three Cys-ligands and a His-ligand. (B) The cluster binding site, showing two hydrogen bonding network, the first between the His-87-ligand, a conserved molecule of water, and Lys-55, and the second between a μ-sulfido ligand, Asp-84, and Ser-77. Proposed hydrogen bonds are represent by dashed black lines. (C) The partial sequence alignment of various eukaryotic mitoNEET homologs. Conserved cluster ligands are highlighted in purple, and conserved residues involved in hydrogen bonding networks around the cluster are highlighted in gold. The cluster-binding loop is underlined.

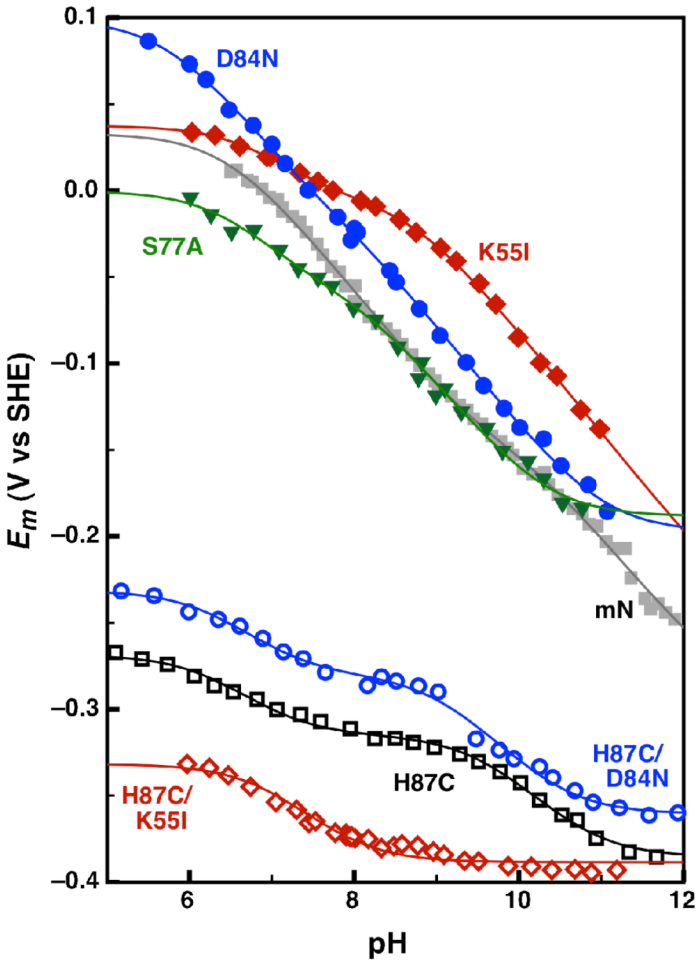

Figure 2.

Comparison of the pH-dependent reduction potential for wild-type and site-directed variants of mitoNEET: wild-type (gray solid squares), H87C (black open squares), K55I (red solid diamonds), D84N (blue solid circles), S77A (green solid triangles), H87C/K55I (red open diamonds), and H87C/D84N (blue open circles). The wild-type, H87C, K55I, D84N, S77A, and H87C/D84N data were each fit to a Nernst equation for 4 pK_a values (Eq 3), while the H87C/K55I data was fit to a Nernst equation for 2 pK_a values (Eq 1).

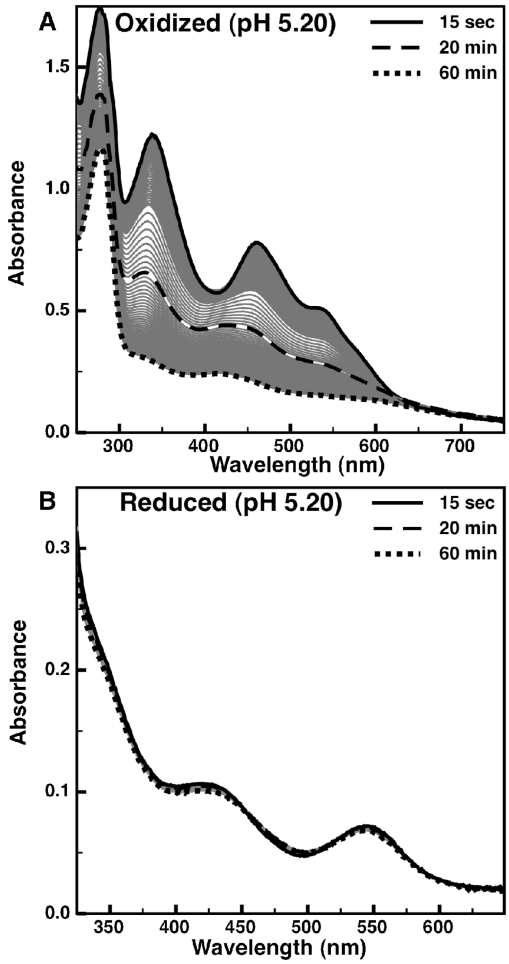

Figure 3.

The time-dependent loss of visible absorption signals for mitoNEET at pH 5.20: (A) oxidized mitoNEET, and (B) reduced mitoNEET. Time-points of 15 second (solid), 20 minutes (dashed), and 90 minutes (dotted) are shown in bold, while intermediate time-points are shown as thin gray traces.

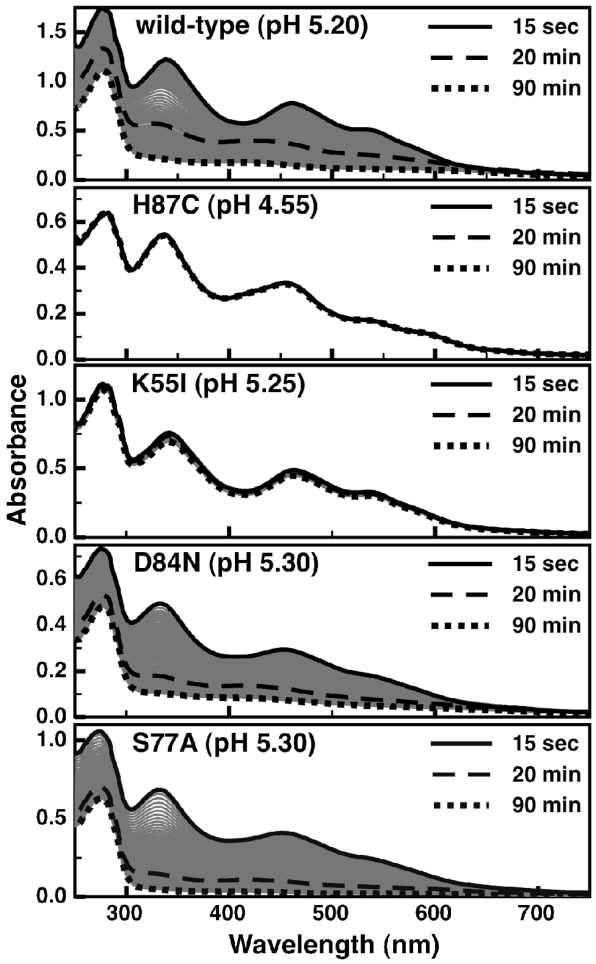

Figure 4.

The time-dependent loss of visible absorption signals for wild-type and site-directed variants of mitoNEET: wild-type at pH 5.20, H87C at pH 4.55, K55I at pH 5.25, D84N at pH 5.30, and S77A at pH 5.30. Timepoints of 15 second (solid), 20 minutes(dashed), and 90 minutes (dotted) are shown in bold, with intermediate time-points shown as thin gray traces.

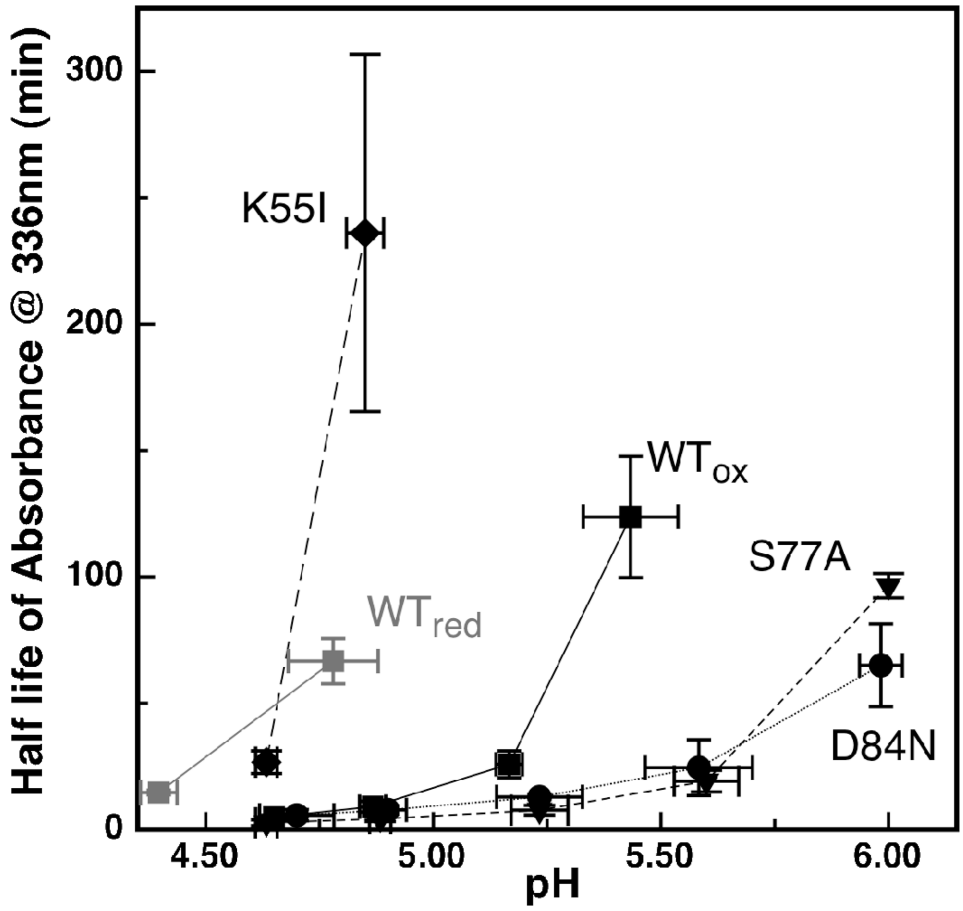

Figure 5.

A comparison of the stability of the [2Fe-2S] cluster optical signals as a function of pH for wild-type and site-directed variants of mitoNEET: wild-type mitoNEET oxidized (black square) and reduced (grey squares), K55I oxidized (diamonds), D84N oxidized (circles) S77A oxidized (triangles). Oxidized H87C is not shown due to its complete stability in this pH range. Plotted is the half-life of the optical signal at 336nm versus pH. Data points and error bars represent the average of three experiments.

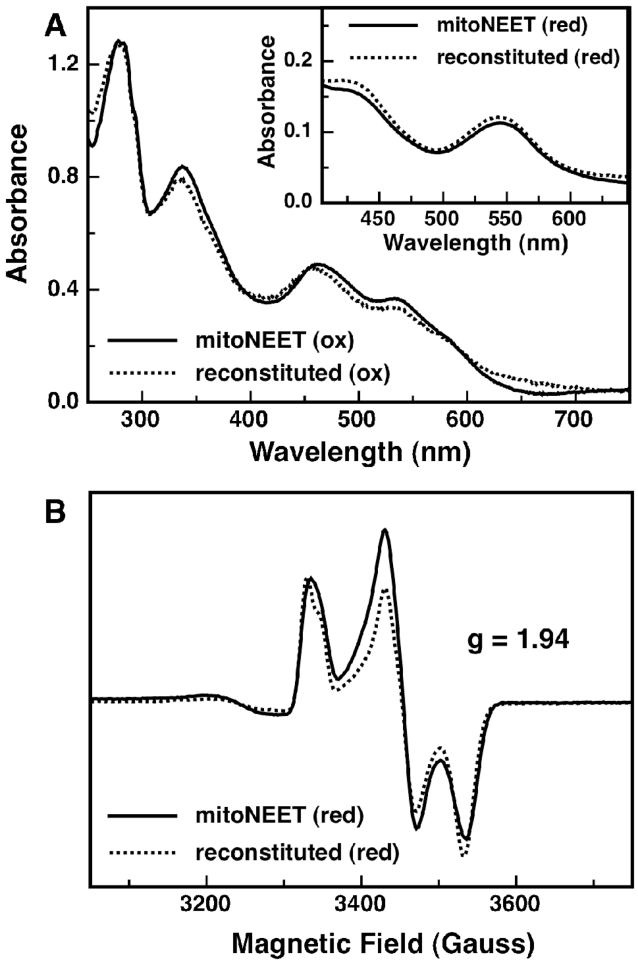

Figure 6.

Spectroscopic characterization of the reconstituted-mitoNEET. (A) Optical spectra of oxidized reconstituted mitoNEET (dotted line) and as-isolated mitoNEET (solid line). Inset: optical spectra of dithionite reduced reconstituted-mitoNEET (dotted line) and as-isolated mitoNEET (solid line). (B) Low temperature (10K) EPR spectra of dithionite-reduced reconstituted-mitoNEET (dotted line) and as-isolated mitoNEET (solid line) measured at 9.24 GHz.

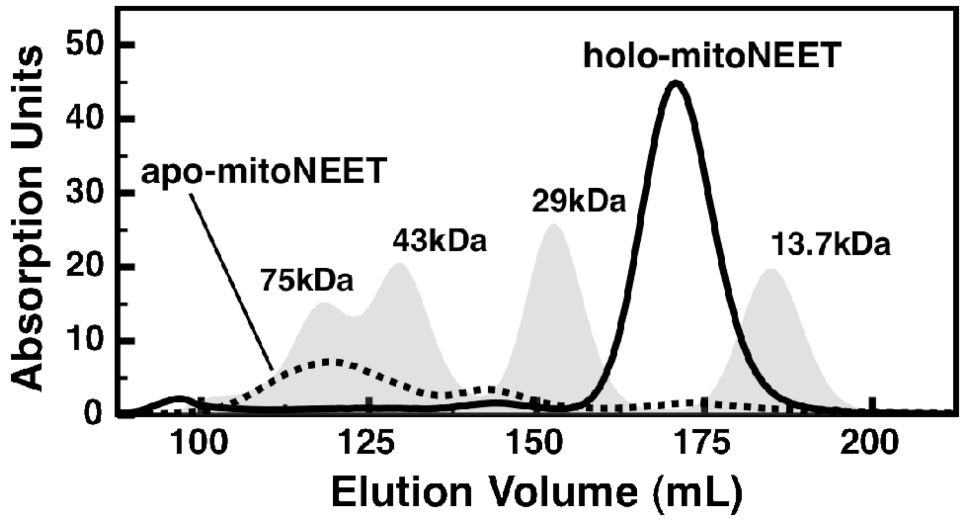

Figure 7.

Size-exclusion chromatograms for wild-type mitoNEET: holo-mitoNEET (solid trace) and apo-mitoNEET (dotted trace). A set of four protein standards is reported for comparison (gray peaks): Ribonuclease A (13.7 kDa), Carbonic Anhydrase (29 kDa), Ovalbumin (43 kDa), and Conalbumin (75 kDa). All chromatograms are calculated from absorbance at 280 nm.

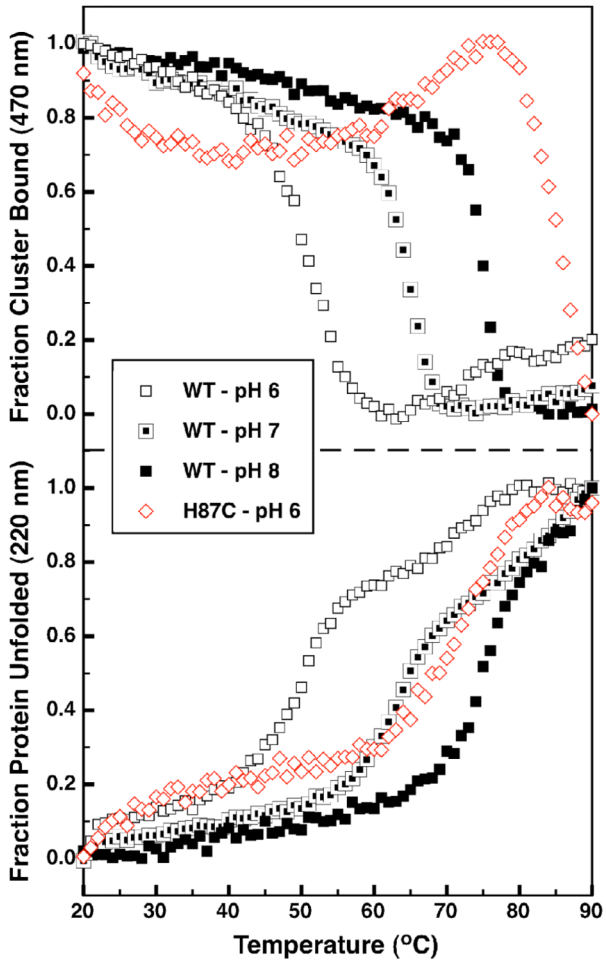

Figure 8.

CD melting curves of the wild-type and H87C variant of mitoNEET. The fraction of bound cluster as monitored by the 470 nm CD band (top panel) and the fraction of unfolded protein (bottom panel) for WT mitoNEET pH 6 (open black squares), pH 7 (half filled black squares), and pH 8 (solid black squares) and for the H87C mutant at pH 6 (open red diamonds).

Table 1

Reduction potentials (E_{acid}) and pK_a values for wild-type and site-directed variants of mitoNEET[a]

	E_{acid} (mV)	pK_{ox1}	pK_{red1}	ΔpK_1	pK_{ox2}	pK_{red2}	ΔpK_2
WT	14±5	6.5±0.1	9.5±0.1	3.0	10.1±0.1	12.6±0.3[b]	2.5
H87C	-267±1	6.3±0.1	7.1±0.1	0.8	9.64±0.1	10.9±0.1	1.2
K55I	37±1	6.7±0.1	7.5±0.1	0.7	8.7±0.1	13±3[b]	4.3
S77A	-11±4	6.4±0.3[b]	7.4±0.4[c]	1.0	8.1±0.2[c]	10.3±0.1	2.2
D84N	86±5	5.7±0.1	7.6±0.3[c]	1.9	7.9±0.3[c]	11.0±0.1	3.1
H87C/D84N	-232±2	6.3±0.1	7.1±0.1	0.8	9.1±0.1	10.4±0.1	1.4
H87C/K55I[d]	-331±2	6.9±0.1	7.9±0.1	1.0			

[a] Unless otherwise indicated the parameters are defined by equation 3. ΔpK is the difference of pK_{red} and pK_{ox}. Error are calculated errors of the fitting process.

[b] Lack of sufficient data at higher or lower ends of the pH range studied, leads to larger uncertainties in the pK_a value.

[c] Larger errors due to inability to properly defining turning points when pK_{red1} and pK_{ox2} are similar.

[d] Parameters are defined for this variant by equation 1.